The Diagram of Feedback Regimes Revisited

Silvano Donati, *Life Fellow, IEEE*, and Ray-Hua Horng, *Senior Member, IEEE*

(Invited Paper)

***Abstract*—We revisit the well-known Tkach and Chraplyvy (T–C) diagram of feedback regimes in semiconductor lasers. Our aim is twofold: first, extending the classification of feedback effects in the T–C diagram to short and long external cavities, and to coherent and incoherent interactions; second and more important, identifying in the diagram feedback phenomena that have been meanwhile studied and developed to noteworthy applications, namely, self-mixing, period-1 and multiperiodicity, intermittency and chaos. We complement the feedback diagram with application regions, so as to describe not only feedback effects detrimental to a laser used as the transmitter of an optical link, but also feedback effects in the weak and strong regime of interaction, developed into applications for instrumentation and communications in recent years.**

***Index Terms*—Chaos, high-level dynamics, laser theory, optical feedback, semiconductor lasers.**

I. Introduction

FOR over 25 years, the diagram of Tkach and Chraplyvy (T–C) [1] has been the reference for describing and classifying feedback effects in semiconductor laser subjected to retroreflections from a remote target [2]–[4]. The T–C diagram identifies five regimes of feedback, and since its publication has become the milestone reference cited in literature and reported in textbooks, the first being the book of Petermann [2].

At the time the T–C diagram was developed, feedback was regarded mainly as a disturbance affecting the performance of linewidth and noise of a laser, and impairing the use of the source in optical fiber communication systems.

Let us consider the basic laser scheme reported in Fig. 1 as the paradigm of feedback. According to the original description [1] of feedback-induced regimes (see Fig. 2), region I is that of the lowest feedback down to -80 dB, yet giving rise to linewidth narrowing or broadening, according to the phase shift 2kL of the optical path external to the laser; region II is up to around -45 dB and involves frequency splitting of the mode, for out-of-phase feedback, and mode hopping; region III is the narrow-range feedback region (about -39 to -45 dB) in which the laser returns to single narrow-line mode; region IV (starting at ≈ -39 dB, independent from distance) is that of satellite modes appearing at multiples of the frequency of relaxation, and of line broadening in a condition termed coherence collapse; region V is observed only at the highest coupling (e.g., ≈ -10 dB, usually requiring antireflection coating of output facet), and is independent of distance too, and brings the laser back to the single-mode oscillation, which now uses the external reflector as the cavity mirror.

The classification in [1] was backed by a theoretical analysis based on the Van der Pol equations with an added delayed term, a formulation with the same structure in the variables E and ϕ of the Lang and Kobayashi equations [5], and one predicting

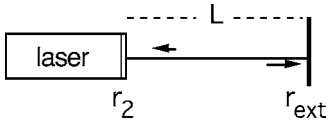

Fig. 1. Schematic of a laser diode subjected to optical feedback from an external reflector (or diffuser) at a distance L, giving back a fraction $r_{\rm ext}$ of the impinging field amplitude. Output mirror (field) reflectance is r_2. Both $r_{\rm ext}$ and r_2 determine the feedback and coupling factors, K and C [see (1) and (2)]. When used in cryptography, the scheme is identified as DOF, whereas it is called SMI when used in phase (and/or amplitude) measurements.

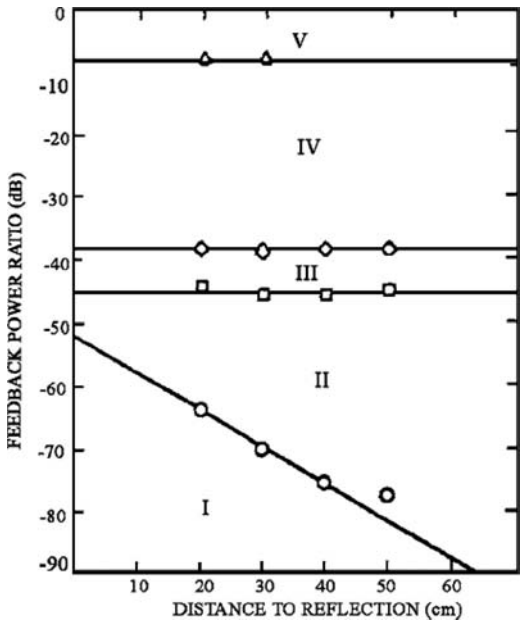

Fig. 2. Original diagram of coupling strength (or back-reflection attenuation) in decibel, versus external cavity length L. According to the original description of Tkach and Chraplyvy [1], region I corresponds to linewidth narrowing or broadening (depending on the phase of feedback), II to line splitting and mode hopping, III return to single-mode narrow-line operation, IV to coherence collapse, V to oscillation on the external cavity. Note that, as the feedback ratio is expressed in decibel, numbers on Y-axis apply both to power attenuation and to electric field amplitude attenuation K (from [1], by courtesy of the IEEE).

Manuscript received October 14, 2012; revised November 17, 2012 and December 10, 2012; accepted December 11, 2012.

S. Donati is with the National Chung-Hsing University, Taichung 402, Taiwan, and also with the Department of Electronics, University of Pavia, 27100 Pavia, Italy (e-mail: silvano.donati@unipv.it).

R.-H. Horng is with the Institute of Precision Engineering, National Chung-Hsing University, Taichung 402, Taiwan (e-mail: huahorng@dragon.nchu.edu.tw).

Digital Object Identifier 10.1109/JSTQE.2012.2234445

mode hopping, multiperiodicity, chaos, and all the high-level dynamics phenomena.

Experiments confirming theoretical findings were conducted on a 1.55-μm distributed feedback laser subjected to a back-reflection from an external (20–400 cm) reflector with adjustable reflectance. The time dependence of power was observed on millisecond scale to reveal mode hopping. The frequency line was measured by an FP scanner with ≈50 MHz resolution to observe frequency splitting, sideband modulations, and linewidth broadening.

In this way, the picture presented by T–C diagram to the user of laser diode as a source for fiber optics communications was complete, and warned that only very weak returns (possibly down to less than -80 dB) can be tolerated with no penalty on noise and linewidth properties of the source.

II. Description of Weak Feedback: The Self-Mixing Regime

In the years that followed, however, high-level dynamic effects in laser diodes have been studied in much more detail. This, from the viewpoint of the evolution and the descriptive character of the oscillation, is represented by field amplitude E and phase ϕ, not just by the linewidth.

Many authors have reported about the time dependence (or time series) of the field amplitude and associated opening and closing bifurcations, and have studied the frequency spectrum (of both field amplitude and frequency fluctuations) and the state diagram (E versus *dE/dt* or $d\phi$/*dt*) as a function of feedback strength K and distance L to the remote reflector.

These studies have pointed out that additional parameters affecting the dynamics are to be considered to fully account for the laser behavior, namely: 1) the optical phase associated with distance, 2kL (mod 2π) when the distance is less than the equivalent relaxation frequency f_2, or $L < c/2f_2$ (this brings about a distinction between *short* and *long* cavities [3]–[6]); 2) the condition of distance L being smaller or larger than the coherence length $L_{\rm coh}$ of the unperturbed source, leading to the two cases of *coherent* and *incoherent* feedback; and 3) of course, all the constitutive parameters (gain, loss, photon and carrier lifetimes, etc.) and above all, the alpha (or linewidth enhancement) factor influencing the actual regime of high dynamical behavior.

Rather than just an undesired disturbance to be avoided, the weak feedback regime (region I of T–C diagram) started to attract interest in 1990s as a hint to measurement applications. Indeed, as feedback affects both amplitude and frequency of the oscillating field, the resulting AM and FM modulations carry signals ΔE and $\Delta\nu$ related to and useful for the measurement of amplitude and phase of the returning field.

The effect on frequency was already noticed by Tkach and Chraplyvy [1]: in region I, they reported linewidth narrowing or broadening, depending on the phase of feedback. They analyzed the linewidth and found that it is a sinusoidal function of the external-path phase 2kL, i.e., $\Delta\nu \approx \sin$ 2kL (see more details later). But the small signal sin 2kL responsible for spoiling the linewidth was never recovered for use in measurements, because it was impressed on the optical carrier and was difficult to demodulate down to electrical frequency.

Unnoticed in the first studies, the effect on amplitude, i.e., the AM of the field E was later realized as quite suitable to develop measurements [7], [11], as the ΔE signal is readily available on the power $P \approx E^2$ emitted by the laser.

The ΔE amplitude signal always accompanies that of frequency $\Delta\nu$, and for weak feedback its dependence is again sinusoidal, of the type $\Delta E \approx E_0 \cos$ 2kL.

Thus, it was realized that feedback-induced modulations, AM and FM, carry driving terms that contain information about the phase $\phi = 2$kL of the external path length as well as of the attenuation $\alpha_{\rm ext} = \Delta E/E_0$ of the returned (echo) field.

The interaction generating AM and FM modulations of the cavity field has been called *self-mixing*, because it comes out as a consequence of the "mixing" of the in-cavity unperturbed field and the weak returned signal, a process which is easily seen to be coherent [7].

Perhaps the most interesting application of self-mixing is in optical measurements, as we can develop a self-mixing interferometer (SMI) based on the AM and FM signals detected by, e.g., a photodiode placed on the rear mirror of the laser (usually the power monitor photodiode can be used to detect the AM). A review of SMI applications to a variety of physical measurands has been recently published [8] and we address the interested readers to it for more details.

At any rate, we can develop an SMI at two different levels of feedback strength: one *very weak* where AM and FM signals are cosine and sine of the external path length 2kL, and we take advantage of a dual-mode source to access also the FM signal, after a down conversion to electrical frequencies by beating with an unperturbed line in dual-mode laser (see [8] and [11] for details). From the sin 2kL and cos 2kL signals, we can unambiguously trace back the phase $\phi = 2$kL, and measure changes of it (for example, in steps of the period $\Delta\phi = 2\pi$). In this way, we can obtain the change or increment of the corresponding target distance ΔL (in the example, in steps of $\Delta L = 2\pi/2k =$ half-wavelength).

An SMI instrument developed under this strategy is classified as a two-channel, incremental measurement of displacement and does not require any phase unwrapping [8].

Of course, we can also make the measurement using just one signal (sin or cos) to retrieve ΔL from $\Delta\phi$, but we shall be able to circumvent the ambiguity associated with the sinusoidal function by means of phase unwrapping, and sometime this is a questionable operation.

Another way we can develop an SMI is at *moderate* feedback, when the AM cosine waveform becomes distorted and the ambiguity can be removed, thanks to the regime of single-switching per period [8]. So, we obtain a one-channel instrument. This happens when another parameter connected to attenuation, namely the *coupling* or C factor, is in the range 1–5. The C factor is defined as

$$C = (1+\alpha^2)^{1/2}\ K(\tau_{\rm ext}/\tau_{\rm in}) \tag{1}$$

where K is field attenuation, explicitly given, in terms of output mirror reflectance r_2 and (remote) target reflectance $r_{\rm ext}$ (see

Fig. 1) by

$$K = \eta_s(1 - r_2^2)(r_{\rm ext}/r_2). \tag{2}$$

In (2), η_s is the mode superposition factor (including the field attenuation $\alpha_{\rm ext}$ on the external path). In (1), $\tau_{\rm ext} = 2\ L/c$ and $\tau_{in} = 2L_{\rm las}n_{\rm las}/c$ are the time of flight of the round trip external (to target) and internal (cavity) to the laser, and α is the linewidth enhancement factor. Inserting the expression of $\tau_{\rm ext}$ in (1) gives

$$C = (\text{const.})\ \text{KL}. \tag{1'}$$

Thus, lines of constant C in the T–C diagram, have a -45° slope, as shown in Fig. 2.

Now, it is found, both from theory and experiments, that as feedback K (or C) is increased, the sin and cos waveforms become progressively distorted (see Fig. 3) until a switching appears in them at $C > 1$, due to the jump of the mode frequency on the next available resonance of the combined three-mirror cavity. This brings about the interesting possibility of removing the phase ambiguity, by looking at the upward or downward switching polarity, which indicates the sign of the λ/2-displacement increments [11] in the range $1 < C < 4.6$.

Based on this scheme, we can build a one-channel SMI digital incremental measurement with half-wavelength resolution using a single interferometric signal, as it has been demonstrated in a number of papers [8], [11].

It is also possible to operate the SMI at even larger C values (e.g., >10), but we then need a more sophisticated algorithm to reconstruct the signal affected by multiple switching [8], [15].

A second, and equally intriguing application, is that we can detect very *weak optical echoes* by looking at the amplitude of the AM signal, either a signal physically different from the laser oscillation or a delayed and attenuated replica of it. This scheme is called injection coherent detector, or self-mix detector (SMD) [8], [9].

When we are operating in the visible and near infrared λ-range, the SMD offers just another possibility with respect to normal coherent photodetection. While not outperforming existing photodetection techniques, the advantage of SMD is the easy way to make a very sensitive back-reflection detector, capable of detecting echoes down to about −90 dB of the outgoing power [7], [9]. On the other hand, the SMD scheme becomes a real breakthrough when we handle signals for which photodiodes are much less efficient or not be readily available, like at THz frequency [9], [33].

Another possibility offered by SMD is that we can dispense with the photodetector, because we find the AM signal already across the laser diode terminals, as anode-to-cathode voltage ΔV. This is due to the self-mixing process in a semiconductor laser, not only affecting field amplitude E, but also carrier concentration N and hence voltage V [9], [33].

In conclusion, as we go back to the T–C diagram, we can redraw the bottom part of it as in Fig. 4, showing that in regions I and II we encounter the self-mixing regime of AM and FM modulations, with a sine/cosine wave dependence on external optical path length at weak feedback and small C, and distorted sinusoid waveforms at increased C, up to the switching promoted by hopping on external mode resonances, in both the AM and FM channels.

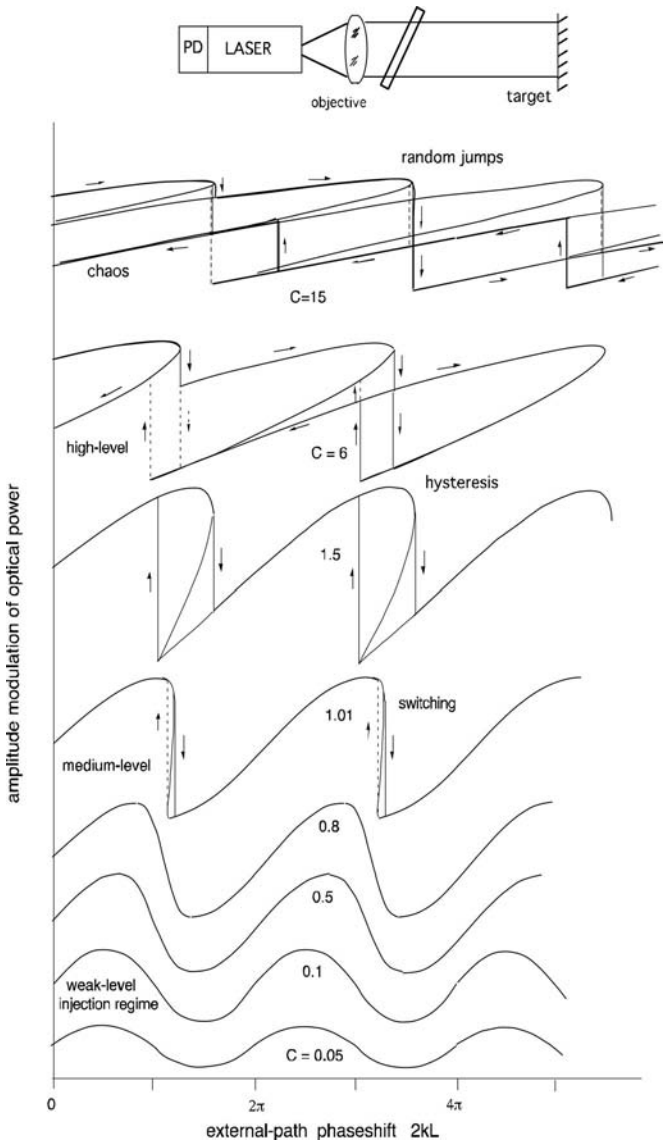

Fig. 3. Diagram shows the waveforms of the AM signal in an SMI at increasing feedback level. Initially, at $C \ll 1$, the AM waveform (and also FM, not shown here) is a sinusoidal function of the external phase shift, like in a normal interferometer, and then it becomes increasingly distorted, with the trailing edge faster than the leading edge ($C < 1$) until a switching appears at the critical value $C = 1$. At larger C, up to about $C = 5$, we find a single switch per period and we can make a single-channel unambiguous count-based SMI. Increasing C further (e.g., $C = 15$), the waveform starts jumping on one ore more external resonances erratically, and the system enters in the chaos regime (adapted from [11]).

From the point of view of applications developed in these regions, we find [8], as depicted in Fig. 5, the two-channel SMI and the injection detection up to about $C \approx 1$, and then the moderate feedback, one-channel SMI starting at $C > 0.3$ and up to $C \approx 10$ with proper signal processing. The self-mixing coherent injection detection (SMD) and the SMI share a common noise floor limitation, typically around −90 dB [9], due to the quantum noise associated with the detected photons [7], [8], [11].

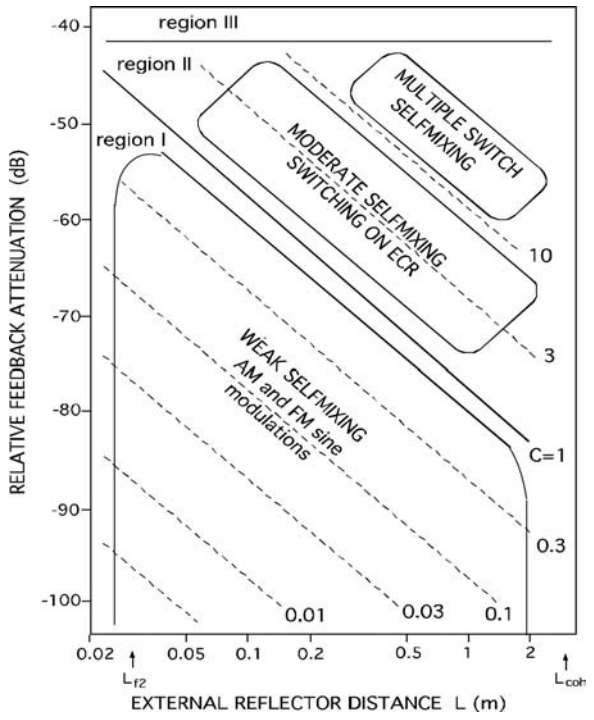

Fig. 4. Revisiting the bottom part of the T–C diagram, across regions I, II, and III: at weak feedback, we find the regime of self-mixing interaction, with AM and FM modulations of the cavity field driven by the external path length phase 2kL. Increasing the feedback at $C = 1$ and larger, we find the moderate feedback regime with switching promoted by external cavity resonance (ECR), initially single (one per period), then multiple for $C > 10$.

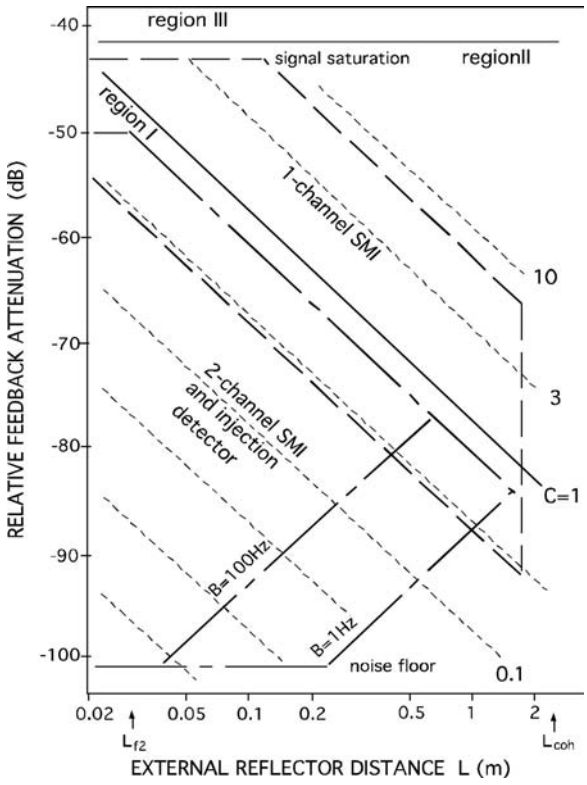

Fig. 5. Applications developed from the regimes reported in Fig. 4: at weak feedback, the 2-channel SMI and the injection (coherent) detector of remote optical echoes (dot-and-dash lines), and at higher feedback, the one-channel SMI interferometer based on half-wavelength switchings (dashed line). Noise floor and quantum noise limit associated with a typical 100-μA photocurrent are indicated [8], for two values of observation bandwidth B.

At the opposite end of high level of signals, we may find a limit due to saturation of the field amplitude (see Fig. 3) and switching of signal waveform, at $C \approx 1$, from about -40 to -30 dB. Last, in Fig. 4, we also draw the limit of maximum distance L of the external reflector, as due to decreased signal amplitude and limit of coherence length $L_{\rm coh}$, a few meters on assuming a linewidth of some tens of megahertz.

III. Theory and Simulations of Feedback Effects

A firm theoretical foundation to study high-level dynamics phenomena is provided by the well-known Lang and Kobayashi (L–K) equations [5]. These equations are the extension of the Lamb's rate equations [10], to the case of a semiconductor laser, when we take account also of the concentration of states N and its dependence on the field amplitude E or density of photons E^2. They are equivalent to the equations used by T–C in their seminal paper [1].

When tested against experiments, the L–K equations provide a remarkably accurate prediction of feedback phenomena and their trends, both at the weak-level SMI level and at the high level of chaos-related dynamics. Thus, it is no wonder that researchers have gained confidence in them and used simulations based on L–K equations extensively for investigating complicated systems, e.g., involving multiple sources or interconnected systems.

The only deviation reported from experiments is a larger than expected linewidth of the laser, reconciled with experiment, as first proposed by C.H. Henry [14], by the introduction of an *a-posteriori* linewidth enhancement factor α. The L–K equations for a laser subjected to feedback [or, a delayed optical feedback (DOF) system as in Fig. 1], are written as follows:

$$\begin{aligned} dE/dt &= \tfrac{1}{2}[G_N(N-N_0) - 1/\tau_p]E + (K/\tau_{\rm in})E(t-\tau_{\rm ext}) \\ &\quad \times \cos[\omega_0\tau_{\rm ext} + \phi(t) - \phi(t-\tau_{\rm ext})] \\ d\phi/dt &= \tfrac{1}{2}\alpha\{G_N(N-N_0) - 1/\tau_p\} \\ &\quad + (K/\tau_{\rm in})E(t-\tau_{\rm ext})/E(t) \\ &\quad \times \sin[\omega_0\tau_{\rm ext} + \phi(t) - \phi(t-\tau_{\rm ext})] \\ (d/dt)N &= J\eta/ed - N/\tau_r - G_N(N-N_0)E^2(t) \end{aligned} \tag{3}$$

where (with the typical values used in simulations)
G_N = modal gain = $8.1{\cdot}10^{-13}$ m^3 s^{-1},
K = fraction of field coupled into the oscillating mode [see (2)]
N = carrier concentration (m^{-3}),
N_0 carrier concentration at inversion = $1.2{\cdot}10^{24}$ m^{-3},
$\tau_{\rm ext} = 2n_{\rm ext}L/c$ = round trip time of external cavity,
$\Phi = 2{\rm kL} = 2n_{\rm ext}k_0$ L external optical phase shift,
L = distance to external cavity reflector
$\tau_{\rm in} = 2n_{\rm las}L_{\rm las}/c$ = round trip time of laser cavity = 5 ps,
τ_p = photon lifetime in laser cavity = 2 ps,
τ_r = carrier lifetime = 2 ns,
α = linewidth enhancement factor (taken $3 - 4.5 - 6$),

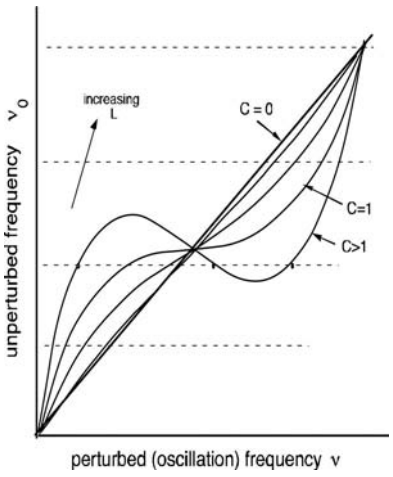

Fig. 6. The diagram of Adler's equation of unperturbed ν_0 versus perturbed frequency ν has a single intersection (one stable solution) for $C < 1$, whereas for $C > 1$ the three intersections (two stable and one unstable), reveals the system is perturbed by the ECR.

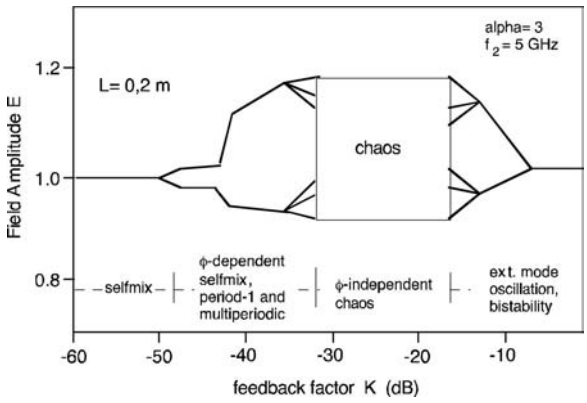

Fig. 7. Sketch of the evolution of dynamic regimes as a function of feedback factor K: self-mixing regime at weak feedback, periodicity and multiperiodicity, chaos and opening closing bifurcations up to the final state of oscillation on the external reflector.

$\omega_0 = k_0 c =$ unperturbed frequency; ($\lambda_0 = 1.55\ \mu$m),
$J\eta =$ pumping current density, and,
$\eta =$ internal quantum efficiency,
$d =$ active layer thickness,
$V =$ active volume $= 8{\cdot}10^{-17}$ m^3.

In the small perturbation regime ($K \ll 1$), we can solve analytically the L–K equations for the amplitude ΔE and frequency $\Delta\nu$ deviations from the unperturbed values, and obtain the cos and sin dependence on 2kL of AM and FM signals [3], [8], [11]:

$$\Delta E/E_0 = K(\tau_p/\tau_{\rm in})\cos 2{\rm kL} \tag{4}$$

and

$$\Delta v = -(1+\alpha^2)^{1/2}(K/\tau_{\rm in})\sin(2{\rm kL} + atan\alpha). \tag{5}$$

Interesting to note, (5) also explains why the linewidth of the perturbed laser is narrowed or broadened depending on the phase of the sine term, i.e., $\Phi = 2{\rm ks} + atan\alpha$, as described in the region I of the T–C diagram.

Letting $\Delta\nu = \nu - \nu_0$ and $k = 2\pi\nu/c$ in (5), we obtain a relationship of unperturbed ν_0 versus perturbed ν frequency of oscillation, and Fig. 6 is the corresponding diagram, also called Adler's diagram because it applies to a very general scheme of a Van der Pol oscillator perturbed by a delayed replica of its own output.

Also, Adler's equation is equivalent to the three-mirror description of the laser feedback scheme, when we write the balance of field at the output mirror [8], [12], [13].

As we can see in Fig. 6, as far as the coupling is small ($C < 1$), there is only one solution for ν (a stable, single oscillating mode). But, at increasing C, the undulation increases in amplitude and for $1 < C < 4.6$ there are three solutions, one unstable (the central one) and two stable, called the external cavity modes [8], [15]. At even larger feedback we get $5, 7, \ldots, n = 2\,C/\pi$ modes, asymptotically. This corresponds to region II of the T–C diagram.

A few more results can be derived analytically from the L–K equations, e.g., threshold current, power-to-current slope, self-mixing waveforms, and high frequency (or modulation) cutoff, etc., but in general most of the high-level dynamic regimes of oscillation can only be studied through numerical simulation of the equations.

The numerical study unveils a number of complex dynamical regimes encountered at increasing K, like bifurcations, period-1 and multiperiodic solutions, chaos, until at high K (approaching unity) oscillation is set by the external cavity.

Experiments nicely confirm [2]–[4] all the theoretical results, with just one adjustment necessary: the already mentioned introduction of the α-factor, in (3), to reconcile experimental linewidth with the theoretical value [13], [14], [34].

Much the same evolution of E as in Fig. 7 is found also at other values of distance L. Exact positions of regimes and bifurcation appearance may change when parameter values are varied, but much the same character is found along a wide range of external reflector distance.

One thing is different at small $L < L_{f2}$, less than the length equivalent $L_{f2} = c/2\ f_2$ of the cutoff frequency of laser modulation f_2: the oscillation regime is dependent upon the phase of the external path length, $\Phi = 2k_0 L$ (mod 2π). So, as L undergoes a change of a wavelength, the regime may change from self-mixing to period-1 to chaos and back [3], [12], [16]. A third variable, phase Φ, should then be introduced in the diagram of K and L to completely describe the system. This circumstance brings about the classification of external cavity and associated regime in *short*, when $L < L_{f2}$, and *long*, when $L > L_{f2}$. For a long cavity, no dependence on Φ (mod 2π) is observed [12], [13].

Another distinction is about feedback coherence. As long as we have $L < L_{\rm coh}$, where $L_{\rm coh}$ is the coherence length of the unperturbed laser, the regime of interaction is *coherent*.

In a semiconductor laser, however, also an *incoherent* return from $L > L_{\rm coh}$ is able to deplete the state concentration N [last term of *dN/dt* in (3)] and drive the system into the high-level dynamics with multiperiodicity and chaos, though less efficiently than a coherent return. In addition to a far-away return ($L > L_{\rm coh}$), incoherent feedback can also be generated by back

reflecting in the cavity a 90°-rotated linear polarization state [20].

In the regime diagrams, we have, therefore, two noteworthy distances: L_{f2} the break point of short-to-long cavity, and $L_{\rm coh}$ the boundary of coherent versus incoherent feedback.

IV. Description of Strong Feedback: Chaos

On increasing the K factor over a certain threshold, the system is driven into a strong interaction characterized by the generation of sidebands that gradually increase in amplitude and number (periodicity and multiperiodicity regimes) until they fill up all the spectrum around the carrier (chaos). These regimes are employed in modern applications of high-level feedback, such as chaos generation and synchronization for optical cryptography, microwave frequency-domain applications, and random number generation.

First question to be considered is the boundary of *weak* versus *strong* interaction regimes. Several papers [16]–[19] have proposed different criteria to assess the boundary, like linewidth analysis, stability of the L–K equations and Lyapunov's exponent. Though findings differ somehow, yet they allow to draw some generally valid conclusions about the "unperturbed" regime, by means of three regions in the K–L diagram, as follows. At large feedback (K up to $\approx 10^{-1}$), it should be $f_2\tau_{\rm ext} < 0.1$–0.2 (or, $L < 0.1$–$0.2\, L_{f2}$); at intermediate strength of feedback, we shall stay at $C < 1$; and at weak feedback (and $L > L_{f2}$) we should keep $K < \approx 2{\cdot}10^{-4}$ (or -74 dB). The asymptotes corresponding to these conditions are plotted in Fig. 8 as dotted lines (the last after a scale break).

Actually, as discussed in a recent paper [6], the unperturbed condition is never reached, because the self-mixing regime is found everywhere in the K–L diagram. We can say that retroreflection leaves the laser source "unperturbed" only by reference to a specific condition, like e.g., limited linewidth broadening as assumed in early works [1], [2], [16]. Indeed, when the self-mixing FM modulation term sin 2kL is small and concealed in the natural frequency line, we can take the source as "unperturbed" from the engineering point of view [6]. This happens when the sidebands created by the self-mixing FM are less than say, $\Delta\nu \approx 10$ MHz, from the optical carrier. Yet in this case, unnoticed in early work, a small amplitude dependence of E from cos 2kL still remains, however of the order of -60 to -40 dB (for $K = -40$ dB or less). The level is small enough to be negligible if the laser is used as a transmitter in communications, while it is well revealed and readily useable in interferometry and echo detection [8].

At higher K, the frequency of sidebands $\Delta\nu$ rapidly increases up to gigahertz and tens-of-gigahertz range, always and only as a self-mixing AM and FM effect excluding any randomness in E and ϕ, and multiperiodicity and chaos effects.

Thus, we suggest the following nomenclature to distinguish the two cases: *weak self-mixing regime* (for the quasi-unperturbed state), and *strong self-mixing regime* for sizable AM and strong FM sideband generations. These add to the well-known cases of *periodicity, multiperiodicity*, and *chaos*.

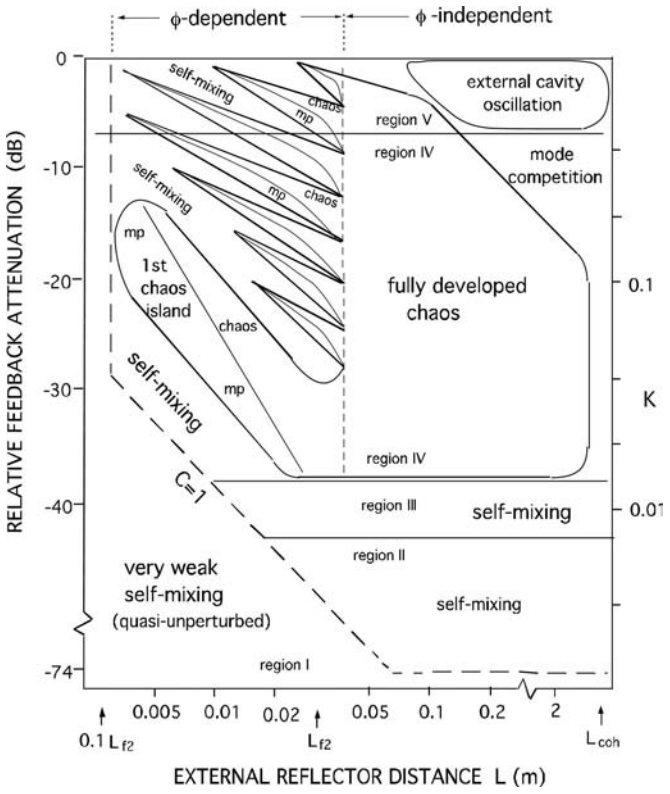

Fig. 8. T–C diagram revisited, across regimes III, IV, and V. Dotted lines are the boundary of "unperturbed" operation, below which only a weak self-mixing interaction takes places, with unnoticeable linewidth broadening. The asymptote at -74 dB is included in the diagram after a Y-scale break. Another scale break, on X-axis, is used to accommodate $L_{\rm coh}$. Increasing K and staying at small L, beyond region III, we find an island of chaos and multiperiodicity. At these short ($L < L_{f2}$) external cavity, the regime is dependent on optical phase $\phi = 2$kL (mod 2π), and it changes from unperturbed (self-mixing) to period-1, to multiperiodic, and chaos, with just a small variation of ϕ. The diagonal thin line in the island gives the relative proportion of chaos and multiperiodicity (mp). On the left side, the island is almost tangent to the unperturbed vertical asymptote (dotted line), and on the right side merges with the fully developed chaos at a length $L \approx L_{f2}$. All around the island, there is a sea of self-mixing regime, this time with sideband frequency in the gigahertz and up to several 10-GHz range. Above the island, we find triangular stripes of multiperiodicity and chaos, ϕ-dependent, which increase in width as L increases and finally merge to the right into the chaos area (thin dotted line). At still higher L, starting from about L_{f2}, we enter a broad area of long-cavity, phase-independent and fully developed chaos. Above about –5 dB, chaos ceases because the system oscillates on the external cavity. Starting from distances of the order of the unperturbed coherence length ($L \geq L_{\rm coh}$), the system exhibits self-locking and unlocking in frequency due to the reflected waves, and bistability in amplitude.

Now, let us consider the upper part of the T–C diagram (see Fig. 8), and go across regions III, IV, and V. At the left side of the diagram, when the external cavity length is small ($L \approx 0.1 L_{f2}$), on increasing K of about 10 dB with respect to the $C = 1$ boundary, we encounter a first island of chaos and multiperiodicity, as described in [6].

We call it first island because it is surrounded by self-mixing (down to the boundary of the long cavity case). Inside the island, the regime of oscillation depends on the optical phase $\Phi = 2k_0 L$ (mod 2π) because the cavity is *short*, and oscillation swings from period-1, to multiperiodic, and chaos, upon just a small variation of Φ.

Of course, we cannot represent the phase-dependent evolution in the K–L diagram of Fig. 8, but in [6] the reader can find the full sequence of waveforms on a 2π cycle for several combinations of parameters K, L, α.

As we move to increased length L, the corresponding K decreases (of about 20 dB/decade) down to about -40 dB, the boundary of T–C region III.

Meanwhile, the relative occurrence in a 2π Φ-cycle of chaos and multiperiodicity is changed, with the chaos proportion increasing steadily up to fill all the available phases. This is (partially) rendered by the thin line running in diagonal in the island. When we reach $L = L_{f2}$ in the island of Fig. 8, the regime is only chaotic, and becomes phase independent, a well-known feature of long external cavity.

Going above the island, we first return to self-mixing regime for a certain range of K values, then, we encounter a number of triangular stripes. These are regions of chaos and multiperiodicity depending on phase Φ, in addition to K and L, and have been described in [6] and [19]. The stripe width is constant across the K-Φ plane, while it increases almost linearly with L and α.

Therefore, in the K–L diagram of Fig. 8, the stripes are triangle shaped and placed along a diagonal. They encompass chaos and multiperiodic oscillation, and are separated by strong-self-mixing regime, with frequency of sideband ranging from several gigahertz up to several 10 GHz. Inside the stripes, we find again a proportion of Φ-dependent chaos and multiperiodicity, increasing from left to right (as indicated by the thin line inside the stripes) and becoming all chaotic as we approach the base of the stripes, at $L = L_{f2}$. Here, the chaos becomes phase insensitive and we have only chaos oscillations in an uninterrupted wide range of K and L.

All the regimes plotted in Fig. 8 are for a linewidth enhancement factor $\alpha = 3$. For other values, from 1.5 to 6, the general description of Fig. 8 still holds. Details (width and number, proportion of chaos, and periodicity) of stripes actually depend on the alpha factor and, in general, with the increase of α the stripes move left or, at constant L, they become thicker and the chaos proportion increases.

At still higher values of K, the chaos regime is suppressed because the system sees an external cavity strong enough to sustain oscillation on its own (see Fig. 8).

Till now, we have tacitly assumed a condition of coherent superposition for the returned field. However, also the case of incoherent feedback interaction is interesting.

An incoherent return actually affects the mode oscillating in a semiconductor laser, because the square-field term E^2 in the last L–K equations [see (3)] depletes the state density N.

Incoherent superposition is found when the return is from a distance $L > L_{\rm coh}$, or when the reinjected mode is orthogonal to a preexisting, in-cavity mode. One way to obtain an orthogonal mode is rotating the state of polarization of returning field by 90°. Ju and Spencer [20] have studied polarization-rotated feedback, which obviously is independent from distance L and phase Φ. At levels of K high enough, they found regime of chaos, self-pulsation, and two-state oscillation. Clearly, no self-mixing regime can be found in incoherent feedback, and at very low K the source is now really unperturbed.

From the point of view of applications developed using high-level dynamics, probably the most actively pursued in recent years, internationally, has been chaos cryptography [3], [4], [12], [21]–[23]. This is a technology based on two fundamental properties of coupled systems: 1) operation in the chaos regime; and 2) synchronization of matched chaos-generating systems.

In principle, we can use either a DOF (single-source system) or an injected coupled laser (ICL, double-source system) to generate chaos [12], but of course the former is preferable from the engineering point of view, because it uses fewer components, is easier to integrate into an integrated photonic circuit (IPC), and does not require two generally tightly matched lasers.

So, the T–K diagram is the adequate means to represent the area of operation of DOF-based systems for chaos cryptography.

The integrated IPC versions of DOF are usually positioned in the upper left corner of the fully developed chaos in Fig. 8. This is because we prefer to incorporate the delay-path L external to the laser as a drift-zone waveguide in the integrated chip, and therefore we wish to keep L as short as possible [24], [25].

A fully developed chaos is found the best for a good synchronization, and thus L will span from L_{f2} (=30 mm from Fig. 8, eventually up to 100 mm, adjustable with the laser bias current), to perhaps a maximum of 3–5 times as much. Considering a $n_{\rm in} = 3.5$ as the effective index of refraction of the waveguide semiconductor material, we will take the guide length L_g in the range $L_g = 10$ to 50 mm.

About the K factor, in the IPC, we may use either a cleaved facet for the reflector ($r_3 = 0.55$ typically) or have the end-face multilayer coated for maximum reflectance and hereafter add an absorber section along the path for the user to trim reflectance. So, the K factor can range from 0.3 to 0.8 in practice.

In Fig. 9, the region covered by IPC versions of chaos DOF for cryptography applications is shown.

Discrete components DOF can work on a somehow wider range of K and L (down to the boundary of regions III and IV and up to $L_{\rm coh}$ in Fig. 9), but size and microphonics effects make them unattractive, after the IPCs have been developed.

Chaos applications to random number generation share much the same area of operation of cryptography and, though relatively recent, can be developed already with specialized IPCs [26], [27].

To attain a high degree of randomness, Sunada *et al.* [27] used an optical-amplifier (OA) boosted ring to return to the laser. The OA compensates the waveguide losses and achieves a net $K = 9.5\%$ coupling coefficient on the long ($n_{\rm in} L_g = 41$ mm) external path. Argyris *et al.* [26] use a conventional F-P external cavity of $n_{\rm in} L_g = 36$ mm and obtain a coupling $K = 1.6$–3.3% that allows to generate a 140 GB/s random data stream.

Other applications of high-dynamic DOF systems are related to microwave tone generation [12], utilizing the period-1 regime; this was the original proposal of Hwang *et al.* [28], based on an ICL scheme. The frequency range covered can span from a few gigahertz up to several times the modulation cutoff frequency f_2.

Further, some applications of chaos to instrumentation have been reported. One is the extension to very high C regime of the basic self-mixing principle [29] (see Fig. 9), by which

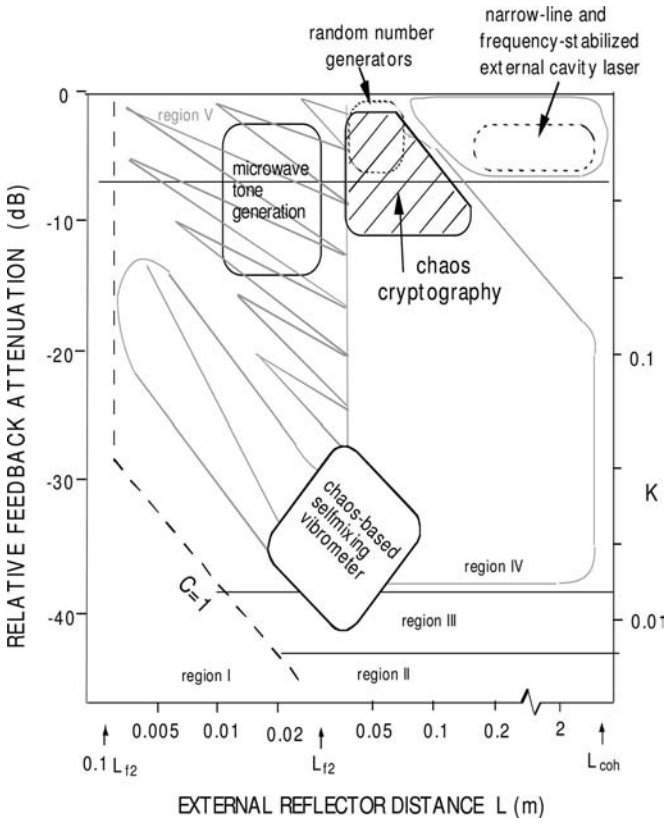

Fig. 9. Preferred areas of operation for some applications using the regimes of Fig. 8: chaos cryptography by DOF (dashed area) random number generation (thin-dot line), microwave tone generation, chaos-based SMI vibrometry, and external cavity frequency stabilized laser.

a demodulated waveform $\Phi = 2kL$ is obtained in place of the normally expected sin Φ. Another proposal [30], [31] is a hint to use a chaos to remove the range ambiguity of the conventional sine-wave modulated telemeter [11], checking the maximum of the autocorrelation function to determine distance; for this feature, the best area of operation is again that of the random number generation.

Last, an application indicated in Fig. 9, though related to suppressing chaos, is the one based on the regime of external cavity oscillation (see the top right corner in Fig. 8) to possibly develop a narrow-line, frequency-tunable laser [32]. This is of course a variant of the well-known external-cavity scheme, the design of which usually starts with a reduced reflectivity r_2 (or an ARC output facet) and a grating as the external target. A three-mirror approach allows us to take account of the nonvanishing reflectivity r_2, and use uncoated chip as the source.

V. Conclusion

We have shown that the well-known T–C diagram of feedback effects is nowadays enriched by a number of interesting phenomena, reported in the literature as the outcome of extensive experiments and simulations that lead to new applications of the high-level regime of coupling or self-coupling in laser diodes. Chaos cryptography and self-mixing interferometry are already established rather well, and others (random number, microwave tone generation, and ranging) are more recent and open the perspective of important new and groundbreaking applications.

References

[1] R. W. Tkach and A. R. Chraplyvy, "Regimes of feedback effects in 1.5-um distributed feedback laser," *IEEE J. Lightw. Technol.*, vol. JLT-4, no. 11, pp. 1655–1661, Nov. 1986.

[2] K. Petermann, *Laser Diode Modulation and Noise*. Dodrecht, The Netherlands: Kluwer, 1991.

[3] K. Ohtsubo, *Semiconductor Lasers: Stability, Instability and Chaos*, 2nd ed. New York: Springer-Verlag, 2009, vol. 111.

[4] D. M. K. Kane and K. A. Shore, *Unlocking Dynamic Diversity—Optical Feedback effects on Semiconductor Lasers*. London, U.K.: Wiley, 2008.

[5] R. Lang and K. Kobayashi, "External optical feedback effects on semiconductor injection laser properties," *IEEE J. Quantum Electron.*, vol. JQE-16, no. 3, pp. 347–355, Mar. 1980.

[6] S. Donati and M. T Fathi, "Transition from short-to-long cavity and from self-mixing to chaos in a delayed optical feedback laser," *IEEE J. Quantum Electron.*, vol. QE-48, no. 10, pp. 1352–1359, Oct. 2012.

[7] S. Donati, *Photodetectors*. Upper Saddle River, NJ: Prentice-Hall, 2000, sec. 8.4.

[8] S. Donati, "Developing self-mixing interferometry for instrumentation and measurements," *Laser Photon. Rev.*, vol. 6, pp. 393–417, 2012.

[9] S. Donati, "Responsivity and noise of self-mixing photodetection schemes," *IEEE J. Quantum Electron.*, vol. 47, no. 11, pp. 1428–1433, Nov. 2011.

[10] M. B. Spencer and W. E. Lamb, "Laser with a transmitting window," *Phys. Rev. A*, vol. 5, pp. 884–891, 1972.

[11] Donati, *Electro-Optical Instrumentation*. Upper Saddle River, NJ: Prentice-Hall, 2004, sec. 4.5.2.

[12] S. Donati and S.-K. Hwang, "Chaos and high-level dynamics in coupled lasers and their applications," *Progress Quantum Electron.*, vol. 36, no. 2/3, pp. 293–341, Mar./May 2012.

[13] K. Petermann, "External optical feedback phenomena in semiconductor lasers," *IEEE J. Sel. Topics Quantum Electron.*, vol. 1, no. 2, pp. 480–489, Jun. 1995.

[14] C. H. Henry, "Theory of spontaneous emission noise in open resonators and its application to laser and optical amplifiers," *IEEE J. Lightw. Technol.*, vol. JLT-4, no. 3, pp. 288–1297, Mar. 1986.

[15] S. Donati, G. Giuliani, and S. Merlo, "Laser diode feedback interferometer for the measurement of displacement without ambiguity," *IEEE J. Quantum Electron.*, vol. 31, no. 1, pp. 113–119, Jan. 1995.

[16] N. Schunk and K. Petermann, "Stability analysis of laser diodes with short external cavity," *IEEE Photon. Technol. Lett.*, vol. 1, no. 3, pp. 49–51, Mar. 1989.

[17] J. Mork, B. Tromberg, and J. Mark, "Chaos in semiconductor lasers with optical feedback: Theory and experiments," *IEEE J. Quantum Electron.*, vol. 28, no. 1, pp. 93–108, Jan. 1992.

[18] P. Spencer, P. Pees, and I. Pierce, "Theoretical analysis," in *Unlocking Dynamic Diversity—Optical Feedback Effects on Semiconductor Lasers*. London, U.K.: Wiley, 2008, ch. 2.

[19] R. J. Jones, P. S. Spencer, J. Lawrence, and D. M. Kane, "Influence of the external cavity length on the coherence collapse regime in laser diodes subject to optical feedback," *IEE Proc. Optoelectron.*, vol. 148, pp. 7–12, 2001.

[20] R. Ju and P. S. Spencer, "Dynamic regimes in semiconductor lasers subjected to incoherent optical feedback," *IEEE J. Lightw. Technol.*, vol. 23, no. 8, pp. 2513–2523, Aug. 2005.

[21] V Annovazzi-Lodi, S. Donati, and A. Scire, "Synchronization of chaotic injected-laser systems and application to optical cryptography," *IEEE J. Quantum Electron.*, vol. 32, no. 6, pp. 953–959, Jun. 1996.

[22] S. Donati and C. Mirasso, "Feature section on optical chaos and applications to cryptography," *IEEE J. Quantum Electron.*, vol. 38, no. 9, pp. 1138–1184, Sep. 2002.

[23] A. Uchida, *Optical Communication with Chaotic Lasers: Applications of Nonlinear Dynamics and Synchronization*. Berlin, Germany: Wiley, 2012.

[24] A. Argyris, M. Hamacher, K. E. Chlouverakis, A. Bogris, and D. Syvridis, "Photonic integrated device for chaos applications in communications," *Phys. Rev. Lett.*, vol. 100, 2008. DOI: 194101.

[25] V. Z. Tronciu, C. Mirasso, P. Colet, M. Hamacher, M. Benedetti, V. Vercesi, and V. Annovazzi-Lodi, "Chaos generation and synchronization using an integrated source with an air gap," *IEEE J. Quantum Electron.*, vol. 46, no. 12, pp. 1840–1846, Dec. 2010.

[26] A. Argyris, S. Deligiannidis, E. Pikasis, A. Bogris, and D. Syvridis, "Implementation of 140 Gb/s true random bit generator based on a chaotic photonic integrated circuit," *Opt. Exp.*, vol. 18, pp. 18763–18768, 2010.
[27] S. Sunada, T. Harayama, K. Arai, K. Yoshimura, P. Davis, K. Tsuzuki, and A. Uchida, "Chaos laser chip with delayed optical feedback using a passive ring waveguide," *Opt. Exp.*, vol. 19, pp. 5713–5724, 2011.
[28] S. K. Hwang, J. M. Liu, and J. K. White, "Characteristics of period-one oscillations in semiconductor lasers subject to optical injection," *IEEE J. Sel. Topics Quantum Electron.*, vol. 10, no. 5, pp. 974–981, Sep./Oct. 2004.
[29] G. Giuliani, S. Donati, M. Passerini, and T. Bosch, "Angle measurement by injection detection in a laser diode," *Opt. Eng.*, vol. 40, pp. 95–99, 2001.
[30] K. Myneni, T. A. Bar, B. R. Reed, S. D. Petel, and N. J. Corron, "High-precision ranging using a chaotic pulse train," *Appl. Phys. Lett.*, vol. 78, pp. 1496–1499, 2001.
[31] F. Y. Lin and J. M. Liu, "Chaotic radar using nonlinear laser dynamics," *IEEE J. Quantum Electron.*, vol. 40, no. 6, pp. 815–820, Jun. 2004.
[32] V. Annovazzi-Lodi, S. Merlo, and S. Moroni, "Power efficiency of a semiconductor laser with an external cavity," *Opt. Quantum Electron.*, vol. 32, pp. 1343–1350, 2000.
[33] J. R. Tucker, J. L. Baque, Y. L. Lim, A. V. Zvyagin, and A. D. Rakic, "Parallel self-mixing imaging system based on an array of vertical-cavity surface-emitting lasers," *Appl. Opt.*, vol. 46, pp. 6237–6246, 2007.
[34] M. Osinski and J. Buus, "Linewidth broadening factor in semiconductor lasers–An overview," *IEEE J. Quantum Electron.*, vol. 23, pp. 9–29, 1987.

Silvano Donati (M'75–SM'98–F'03–LF'09) is a Visiting Professor at National Chung-Hsing University, Taichung, Taiwan, and a Lecturer in optoelectronics in the Department of Electronics, University of Pavia, Pavia, Italy, where he was a Chair professor from 1980 to 2010. He has authored or coauthored about 300 papers and holds a dozen patents. He has introduced self-mixing interferometry and chaos-shift-keying cryptography, the topics covered in his Distinguished Lecture talk given in 21 LEOS (now IPS) Chapters in two terms, 2007/2008 and 2008/2009. He is the author of two books, *Photodetectors* (Prentice-Hall, 1999) and *Electro-Optical Instrumentation* (Prentice-Hall, 2004) the latter translated into Chinese (Jiao Tong University Press).

Dr. Donati was the Founder in 1996 and the first Chairman from 1997 to 2001 of the Italian LEOS Chapter, LEOS VP Region 8 Membership from 2002 to 2004, LEOS Board of Governors Elected member from 2004 to 2006), and the Chairman of the IEEE Italy Section from 2008 to 2009. He acted as the Guest Editor of Special Issues, on Fiber Optics and Passive Components (JSTQE Sep. 1999), on Laser Interferometry (*Journal of Optics* A 1998 and 2002, Optical Engineering 2001), and Feature Issues of IEEE JOURNAL QUANTUM ELECTRONICS, Sept. 2002, on Optical Chaos and Applications to Cryptography, and on Photodetectors (Aug. 2004). He has been a Visiting Professor at several Universities, National Taiwan University, Taipei, 2005, Sun Yat Sen (2007, 2008, and 2010), and National Cheng Kung University, Tainan, 2012. He is a Fellow of the Optical Society of America, and Meritorious Member of AEIT (Italian Electrical and Electronic, Engineers Association).

Ray-Hua Horng (M'07–SM'11) received the B.S. degree in electrical engineering from National Cheng Kung University, Tainan, Taiwan, in 1987, and the Ph.D. degree in electrical engineering from National Sun Yat-Sen University, Kaohsiung, Taiwan, in 1993.

She has done work in the field of III–V compound materials by MOCVD as an Associate Researcher at Telecommunication Labs/MOTC, China. She is currently the Dean of the Institute of Innovation Industry School and a Professor of the Institute of Precision Engineering, National Chung-Hsing University, Taichung, Taiwan. She also is the NSC Optoelectronic Division Coordinator. She has authored or coauthored more than 100 technical papers and holds more than 60 patents in her fields of expertise. Her main research interests include solid-state EL devices, III–V optoelectronic devices, high dielectric materials for DRAM applications, nano-surface treatment by natural lithography and GaN nano-wire growth. In 2000, she vitalized her research on high-brightness LEDs with mirror substrate into practical mass products that enable high-power LEDs.

Dr. Horng received numerous awards recognizing her work on high-brightness LEDs. She has been awarded by the Ministry of Education of Taiwan for Industry/University Corporation Project in 2002, by the National Science Council of Taiwan for the excellent technology transfer of high-power LEDs in 2006, 2008, 2009, 2010, and 2011, by Chi Mei Optoelectronics for the first prize of Chi Mei Award in 2008, and by 2007 IEEE Region 10 Academia-Industry Partnership Award.